Materials Today Bio 25 (2024) 100980

Contents lists available at ScienceDirect

Materials Today Bio

journal homepage: www.journals.elsevier.com/materials-today-bio

Niclosamide - encapsulated lipid nanoparticles for the reversal of pulmonary fibrosis

Yan Yu [a,1], Hongyao Liu [b,1], Liping Yuan [a], Meng Pan [a], Zhongwu Bei [a], Tinghong Ye [b,**], Zhiyong Qian [a,*]

[a] Department of Biotherapy, Cancer Center and State Key Laboratory of Biotherapy, West China Hospital, Sichuan University, Chengdu, Sichuan, 610041, China
[b] Department of Gastroenterology and Hepatology, Sichuan University-University of Oxford Huaxi Joint Centre for Gastrointestinal Cancer and Frontiers Science Center for Disease-Related Molecular Network and State Key Laboratory of Biotherapy, West China Hospital, Sichuan University, Chengdu, Sichuan, 610041, China

ARTICLE INFO

Keywords:
Pulmonary fibrosis
Ncl-Lips
Immune microenvironment
Reversal
EMT

ABSTRACT

Pulmonary fibrosis (PF) is a serious and progressive fibrotic interstitial lung disease that is possibly life-threatening and that is characterized by fibroblast accumulation and collagen deposition. Nintedanib and pirfenidone are currently the only two FDA-approved oral medicines for PF. Some drugs such as antihelminthic drug niclosamide (Ncl) have shown promising therapeutic potentials for PF treatment. Unfortunately, poor aqueous solubility problems obstruct clinical application of these drugs. Herein, we prepared Ncl-encapsulated lipid nanoparticles (Ncl-Lips) for pulmonary fibrosis therapy. A mouse model of pulmonary fibrosis induced by bleomycin (BLM) was generated to assess the effects of Ncl-Lips and the mechanisms of reversing fibrosis *in vivo*. Moreover, cell models treated with transforming growth factor β1 (TGFβ1) were used to investigate the mechanism through which Ncl-Lips inhibit fibrosis *in vitro*. These findings demonstrated that Ncl-Lips could alleviate fibrosis, consequently reversing the changes in the levels of the associated marker. Moreover, the results of the tissue distribution experiment showed that Ncl-Lips had aggregated in the lung. Additionally, Ncl-Lips improved the immune microenvironment in pulmonary fibrosis induced by BLM. Furthermore, Ncl-Lips suppressed the TGFβ1-induced activation of fibroblasts and epithelial–mesenchymal transition (EMT) in epithelial cells. Based on these results, we demonstrated that Ncl-Lips is an efficient strategy for reversing pulmonary fibrosis via drug-delivery.

1. Introduction

Pulmonary fibrosis (PF), characterized by the excessive deposition of extracellular matrix and myofibroblast accumulation, is an unpredictable and serious progressive lung disease [1–3]. The development of pulmonary fibrosis in a changing living environment is affected by smoking, microbial infection, genetic factors and environmental factors [4]. Approximately 5 million people suffer from PF worldwide and the median survival period is reported to be only 2–5 years, which is a potentially life-threatening situation. Moreover, clinical studies have shown that PF is related to coronavirus disease 2019 (COVID-19) [5]. Pirfenidone and nintedanib are currently the only two antifibrotic drugs approved for the treatment of PF. Both drugs have multiple adverse effects and are largely palliative [6]. There is an urgent need for new therapeutic strategies for slowing or possibly reversing PF progression.

Niclosamide was the FDA (the U.S. Food and Drug Administration) approved anthelminthic drug in 1982. It is also a multifunctional and promising drug that has been shown to be safe [7,8]. Although niclosamide therapy is extremely safe and tolerable, its clinical applicability has been limited by its poor pharmacokinetic profile following different routes of administration [9]. Niclosamide has been shown to have pleiotropic anticancer effects and macrophage-reprogramming/immunomodulating properties [10]; in particular, niclosamide is a powerful signal transducer and activator of transcription 3 (Stat3) and Notch inhabitor [11–13]. In addition, some clinical studies are currently evaluating the efficacy of niclosamide in relation to treating cancer or COVID-19 [14–16]. Previous studies have shown the anti-pulmonary fibrosis effect of niclosamide [1]. Niclosamide has been shown to mitigate pulmonary fibrosis both *in vitro*

* Corresponding author.
** Corresponding author.
E-mail addresses: yeth1309@scu.edu.cn (T. Ye), anderson-qian@163.com (Z. Qian).
[1] Yan Yu and Hongyao Liu contributed equally to the manuscript and should be considered co-first authors.

https://doi.org/10.1016/j.mtbio.2024.100980
Received 13 October 2023; Received in revised form 8 January 2024; Accepted 25 January 2024
Available online 16 February 2024

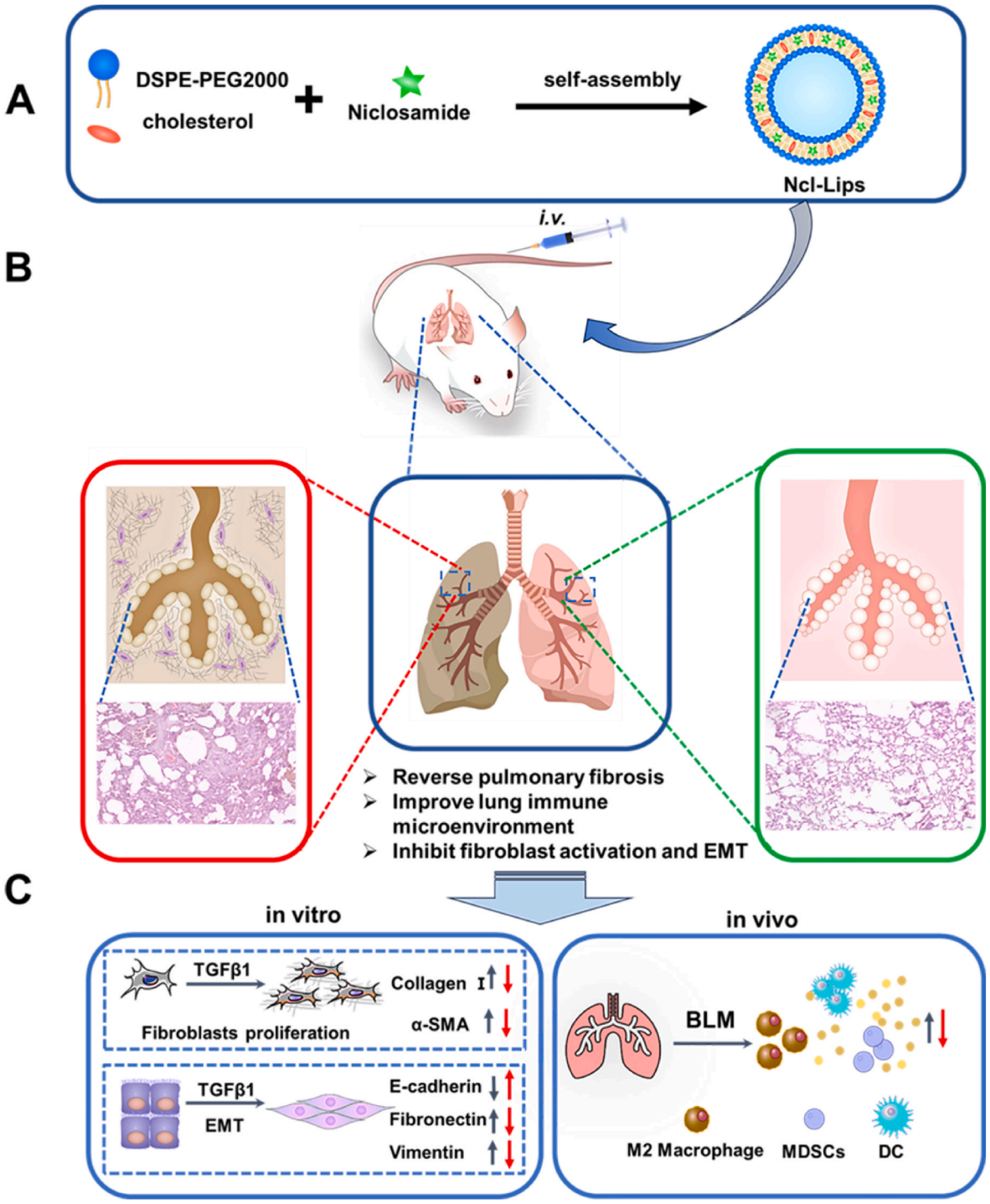

Fig. 1. Schematic illustration of the preparation and expected basic mechanism through which Ncl-Lips reverse pulmonary fibrosis. (A) An illustration of the Ncl-Lips sample preparation process. (B) Diagram illustrating the expected effect of Ncl-Lips *in vivo*. (C) The expected mechanism of action of Ncl-Lips *in vitro* and *in vivo* (The red arrows represent after treatment of Ncl-Lips). (For interpretation of the references to colour in this figure legend, the reader is referred to the Web version of this article.)

and *in vivo* through the suppression of epithelial−mesenchymal transition (EMT), matrix proteins, Wnt/β-catenin signaling, oxidative stress, MAPK/Nf-κB signaling and Stats [17–20]. Therefore, niclosamide is a class II drug that has several drawbacks, such as low solubility and extremely low bioavailability [21]. Nanoparticles have become the focus of drug research for drugs with poor bioavailability [22]. In previous research, we found that niclosamide loaded nanoparticles (Ncl-NPs) could inhibit and reverse established pulmonary fibrosis [15]. However, the use of micelles in this method is limited because of clinical application.

With the development of nanotechnology, there are numerous nanocarriers, such as liposomes, nanoparticles, polymeric micelles, nanogels, carbon-based materials, and metal nanocarriers. As reported, the enhanced biocompatibility of organic nanocarriers contributes to their significant potential for clinical translation. However, inorganic materials exhibit diminished biosafety [23]. Among the several drug-loaded nanocarriers, lipid nanoparticles (Lips) are major drug delivery systems that can be used to control drug distribution and release. Lips can also enhance biocompatibility, reduce side effects and increase

the ease of industrialization [24,25]. An increasing number of groups have used Lips as targeted delivery platforms for small molecules, peptides, and genes [26,27]. Herein, we designed and developed niclosamide-encapsulated lipid nanoparticles (Ncl-Lips), which are safe intravenous delivery systems. Ncl-Lips were chosen because they are easy to prepare and stable (Fig. 1). We found that Ncl-Lips could reverse pulmonary fibrosis *in vivo*. Furthermore, Ncl-Lips fundamentally reverses the pulmonary fibrosis microenvironment and inhibits EMT process in lung epithelial cells. In summary, we report that Ncl-Lips may constitute a new, therapeutic and simple strategy for treating pulmonary fibrosis.

2. Materials and methods

2.1. Materials

Cholesterol was purchased from shanghai Yuanye Bio-technology Co., Ltd. Distearoyl phosphatidylethanolamine DSPE-PEG2000 was acquired from Xi'an ruixi Biological Co., Ltd. Ethanol, NaOH, HCl and dimethyl sulfoxide (DMSO) were purchased from Shanghai Macklin Biochemical Technology Co., Ltd. Cell count kit-8 (CCK-8) was acquired from Baoguang Biotechnology Co., Ltd. (Chongqing, China). The niclosamide (Ncl) was acquired from Xiya Reagent Company (Shandong, China) and Bleomycin sulfate was purchased from Macklin Inc. (Macklin, Shanghai, China). TGFβ1 was acquired from Novoprotein (Shanghai, China). The anti -β-actin was obtained from ZSGB-BIO Biotech (Beijing, China). Collagen I (ET1609-68) and α-SMA (ET1607-53) were obtained from HUABIO (Hangzhou, China). PE-CD11b-, APC-CD206-, FITC-CD11b-, FITC-Gr-1-, PE-F4/80-, APC-MHC II-, and FITC-CD11c-conjugated antibodies were obtained from Biolegend (San Diego, CA, USA). Fibronectin (ab32419), E-cadherin (ab76055) and vimentin (ab20346) were purchased from Abcam (Cambridge, MA, USA).

2.2. Synthesis and characterizations of Ncl-Lips

Lipid nanoparticles was prepared according to the previous study with slight modification [28]. To put it briefly, 10 mg niclosamide in 1 mL DMSO solution was lyophilized to form fixed fluffy medication. 28 mg DSPE-PEG2000 and 1.9 mg cholesterol were mixed in 500 μL ethanol by gentle ultrasonic dispersion. Then 500 μL of 0.1 M NaOH solution was added to the above solution. Then the solution was gently shaken for a few minutes to disperse. The mix was diluted with 9 mL ultrapure water with micro-injection pump within 3 min. The last step was neutralized with 0.1 M HCl. The resulting pH (neutral) was verified with pH meter. TEM images of liposomes were carried out with the TEM system (JEOL JEM 2100F). The Ncl-Lips were negatively stained with 2% uranyl acetate by using the copper grids. The zeta-potential and size of Ncl-Lips were measured with a Malvern Zetasizer Nano (Malvern, England). Ultraviolet–visible (UV–vis) spectroscopy were characterized by ultraviolet–visible spectrophotometer (UV−2600, Shimadzu, Japan).

2.3. In vitro drug release study

The concentration of niclosamide were used to assess the loading ability of Ncl-Lips. The content of niclosamide in Ncl-Lips was used to qualitatively analyze using HPLC methods. HPLC profiles were performed by reverse-phase HPLC (RP-HPLC, Agilent-1260, USA) using a C18 column (4.6 mm × 250 mm, 5 μm). In short, the column was eluted with buffer C (0.1% formic acid in acetonitrile) and buffer D (0.1% formic acid in water) and the absorbance at 332 nm was monitored at a flow rate of 1.0 mL/min: starting composition 20% C, linear gradient from 80% B from 0 ~ 2 min, hold at 95% C from 2 ~ 7 min followed by re-equilibration at 5% D for 5 min hold at 95% C from 7 ~ 18 min followed by re-equilibration at 5% D for 11 min. The determination of the encapsulation efficiency (EE) and drug loading (DL) of the liposomes was conducted through HPLC measurements based on Equations (1) and (2), respectively.

$$EE(\%) = \frac{mass\ of\ drug\ encapsulated\ in\ Lips}{mass\ of\ drug\ initially\ added} \times 100\% \quad (1)$$

$$DL(\%) = \frac{mass\ of\ drug\ encapsulated\ in\ Lips}{mass\ materials\ and\ drugs\ of\ Lips} \times 100\% \quad (2)$$

2.4. Drug release assay

1 mL of Ncl-Lips solution was introduced into pre-treated dialysis bags (MW: 1000 kDa), accordingly, which was merged into the 20 mL 0.01 M PBS with 1% Tween 80 (v/v) in BD tube. The concentration of drugs was determined by shaking with speed of 100 rpm at 37 °C for 0.5 h, 1 h, 2 h, 4 h, 8 h, 12 h, 24 h, 48 h, 72 h, 96 h, 120 h, and 144 h. Sampling volume was 1 mL, which was immediately replaced with the same amount of 37 °C fresh 0.01 M PBS with 1% Tween 80 (v/v). Detection was taken by HPLC (Agilent-1260).

2.5. Animal studies of pulmonary fibrosis

Male C57BL/6 mice aged 6–8 weeks and weighing 18–20 g were used. The animals were purchased from Beijing HFK Biotechnology Co., LTD. (Beijing, China). Mice are isolated, acclimated for 2 weeks, animal tests comply with the guidelines for Animal Research: *In Vivo* Experiment Report (ARRIVE), and comply with the National Institutes of Health (NIH) guidelines NO.8023. All animal experimental procedures were approved by the Institutional Animal Care and Treatment Committee of Sichuan University in China (New Permit Number: 20220531048). Pulmonary fibrosis was induced by ~2 mg/kg bleomycin (BLM). The mice were randomly divided into four groups (n = 8), including sham + saline group (*i.v.*); BLM + blank-Lips (*i.v.*); BLM + Ncl-Lips group (NL-H, 2 mg/mL, *i.v.*); BLM + Ncl-Lips group (NL-L, 1 mg/mL, *i.v.*), and BLM + Ncl group (5 mg/kg, *i.p.*), from the 10th day after endotracheal injection of bleomycin. A control group (sham) was given the same volume of saline. Doses were administered every two days intervals, initiated day 10 and discontinued on day 22. On day 22, all mice were sacrificed and their tissues were collected for subsequent evaluation.

2.6. Hydroxyproline assay

The content of hydroxyproline in the lungs of mice was measured with the hydroxyproline measuring kit (Jiancheng Bioengineering, Nanjing). 30 mg (wet weight) of lung tissue was precisely weighed, and the pH was subsequently adjusted to neutral following the process of cracking. After active carbon adsorption centrifugation, the supernatant was taken and the absorptivity of the sample at 550 nm was measured by UV–visible spectrophotometer.

2.7. Serum biochemistry

Serum was collected from mouse eyeballs after centrifugation. Biochemical indicators of alanine aminotransferase (ALT), aspartate aminotransferase (AST), total protein (TP2), uric acid (UA), high-density lipoprotein 3 (HDCL3) and high-density lipoprotein 4 (HDCL4) were tested by a cobas 311 analyzer (Roche diagnostics) according to guidelines provided by the manufacturer.

2.8. H&E and Masson's trichrome staining

Animal tissues were fixed with 4% paraformaldehyde for 72 h, washed with milli-Q water, dehydrated with gradient alcohol and xylene in proper order. These tissues were embedded with paraffin wax and subsequently sliced into 4 μm sections in tnickness. H&E dyeing and Masson tri-color dyeing (BASO, BA-40798) were applied. The ashcroft

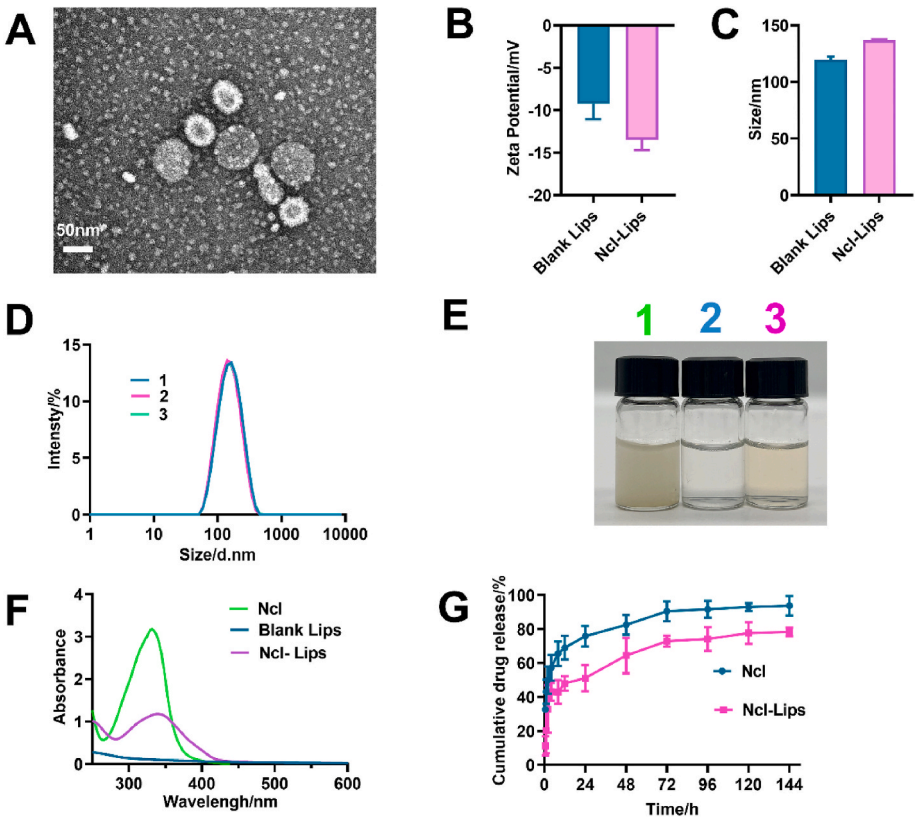

Fig. 2. Characterization of the liposomes. (A) TEM image of Ncl-Lips. (B) Average particle sizes of Ncl and Ncl-Lips. (C) Zeta potentials of Ncl and Ncl-Lips. (D) Size distribution of Ncl-Lips. (E) Appearance picture of 1) Ncl dispersed in water, 2) blank Lips and 3) Ncl-Lips. (F) UV–vis spectra of Ncl, blank Lips and Ncl-Lips. (G) *In vitro* drug release monitoring of Ncl and Ncl-Lips.

score was used to assess the severity of pulmonary fibrosis, and the collagen volume fraction was analyzed with image J software to quantify collagen deposition. H&E staining was used to analyze major tissues except lung to evaluate systemic organotoxicity.

2.9. Flow cytometry

Small amount of lung tissue was sliced into fragments from the identical part and digested with collagenase IV at 37 °C for at least 1.5 h. After centrifugation, the supernatant was discarded and re-suspended with PBS. After precipitation, the supernatant was taken and cultured with different antibodies for 30 min to label multiple immune cells. The results were detected and analyzed using FACS Canton II NovoCyte instrument manufactured by ACEA.

2.10. Pharmacokinetics and biodistribution studies in vivo experiments

The *in vivo* pharmacokinetic tests and biodistribution of Ncl and Ncl-Lips were carried out on the SD female (~200 g, each group consisted of three rats). A dosage 1.0 mg/kg of Ncl or Ncl-Lips was administered intravenously to each rat within distinct groups via the tail vein. Rats were sacrificed at predetermined time points. The brain, kidneys, liver, lungs, and spleen were obtained from each rat and subsequently washed with 1 × PBS buffer solution (pH 7.4). Additionally, blood samples were obtained from each group of rats by extracting it from main abdominal vein. The acquired tissues and blood samples were then preserved at a temperature of −80 °C until they were subjected to analysis. Extraction of Ncl from tissues and blood of rats was performed according to the method of our group research with minor modifications [29]. Finaly, samples were quantified using ultra-performance liquid chromatography-mass spectrometry (UPLC−MS/MS) by Sichuan Greentech Bioscience Co., Ltd.

2.11. Cell lines and cell culture

NIH/3T3 cell line (derived from mouse embryonic fibroblasts) was obtained from Zhong Qiao Xin Zhou Biotechnology Co., ltd. A549 (Human alveolar epithelial cells) and BEAS-2B (Human Bronchial Epithelioid cells) were obtained from American Type Culture Collection (ATCC) (Rockville, MD, USA). The normal human liver cell line (LO2) was acquired from the Cell Bank of the Chinese Academy of Science. Vero cell line was derived from preservation of laboratory. The cells were cultured in Dulbecco's modified Eagle's medium containing 10% foetal bovine serum(v/v) and 1% antibiotics (penicillin and streptomycin) under 5% CO_2 atmosphere at 37 °C.

2.12. Cell viability determination

CCK-8 assay was employed to assess cellular proliferation in NIH-3T3, A549, BEAS-2B, Vero and LO2 cell lines *in vitro*. Briefly, the cells were initially cultured in 96-well plates at a density of 1500 cells/well overnight. Subsequently, fresh medium containing Ncl or Ncl-Lips (0–80 μg/mL) was added. Simultaneously, we established blank Lips to eliminate its own toxic interference. After 72 h of incubation, 10 μL of CCK-8 was added to each well. Finally, the absorbance at the wavelength of 450 nm was measured using microplate reader (Multiskan FC, Thermo Scientifific).

2.13. Immunofluorescence analyze

NIH-3T3, A549 and BEAS-2B cells were separately inoculated into 24-well plates at a density of 1000 cells per well. Following cell adhesion, they were starved in serum-free DMEM medium for 6 h. Subsequently, they were treated with Ncl/Ncl-Lips (5 μg/mL) and TGFβ1 (5 ng/mL) for 24 h, respectively. The cells were rinsed with PBS, fixed and

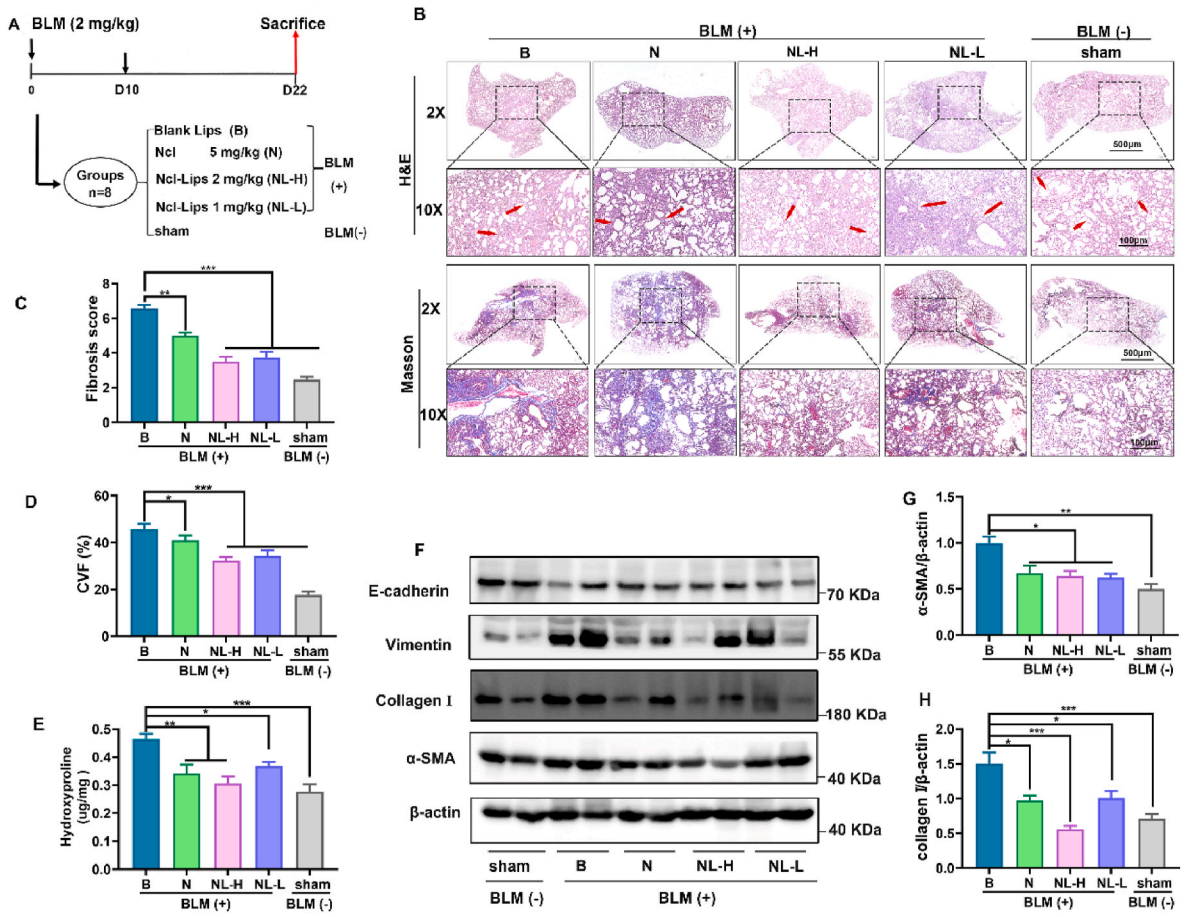

Fig. 3. The therapeutic effect of Ncl-Lips on a pulmonary fibrosis model induced by BLM. (A) Schematic illustration depicts the Ncl-Lips therapeutic model in mice *in vivo*. (Ncl-Lips group 2 mg/mL (NL-H) and Ncl-Lips group 1 mg/mL (NL-L). (B) Representative images of lungs analyzed by H&E staining and Masson's trichrome staining. Scale bars: 500 and 100 μm. (C) Assessment of pulmonary fibrosis according to Ashcroft scoring in each group. (D) Quantification of the collagen volume fraction (CVF) based on Masson's trichrome staining. (E) Hydroxyproline levels in the lung tissue of each group. (F–H) Western blot analysis (F) and statistical analyses of a-SMA (G), collagen I (H) and β-actin in lung homogenates from mice. All the data are expressed as the means ± SDs. n = 3–5, $^{*}P < 0.05$; $^{**}P < 0.01$, and $^{***}P < 0.001$.

permeabilized with methanol-acetone (1:1) and blocked with 5% BSA, then incubated overnight with specific primary antibody at 4 °C. After the cleaning procedure, cells were subjected to an incubation period of 1.5 h with specific secondary antibodies, as well as a 10 min exposure to DAPI. Subsequently, the cells were sealed using an anti-fluorescence quencher. A laser confocal microscope (Zeiss) was used to capture the images. Finally, ImageJ and Graphpad prism 8.0 were used for image analysis, data treatment, and statistical analysis.

2.14. Morphological experiment and wound migration assay

The cells were seeded onto 6-well culture plates and subsequently subjected to scratching using a pipette tip when the cells reached 80% fusion. Rinse gently with free serum DMEM and TGFβ1 or the drug was introduced into the corresponding well subsequently and subjected to 24 h culture period. Photographs were taken through a microscope to record each group of photos at 0 h and 24 h. Finally, the ImageJ software was utilized to assess the proportion of the initial width by quantifying the width of the scratch.

2.15. Western blot analysis

The tissues and cells were lysed utilizing Ripa lysis buffer and quantified using BSA. About 50 μg of total protein was isolated through SDS-PAGE gel and subsequently transferred to polyvinylidene fluoride (PVDF) membrane (Merck Millipore). Then the membrane was obstructed with 5% skim milk for 1 h, followed by incubated with specific primary antibody at 4 °C overnight, subsequently incubated with secondary antibody poetry for 1.5 h, and detected were carried out via ChemiScope 6200 Touch (CLiNX). Finally, Densitometric analysis of images was performed using ImageJ software.

2.16. Statistical analysis

In each of experiments, at least three replicates were conducted and the results were presented as means ± standard deviations (SDs) and P-values were determined by two-tailed Student's t-test for comparison of two groups, and among multiple groups were assessed through one-way ANOVA followed by Tukey's test. Statistical significance was defined as: $^{*}P < 0.05$, $^{**}P < 0.01$, and $^{***}P < 0.001$.

3. Results

3.1. Synthesis and characterization of Ncl-Lips

Niclosamide has a low bioavailability and is fundamentally characterized by its limited solubility in water. These disadvantages restrict its application. Ncl-encapsulated lipid nanoparticles (Ncl-Lips) were prepared in this study which aimed to enhance the solubility and biocompatibility of Ncl. TEM analysis (Figure S1, 2A) revealed that the round

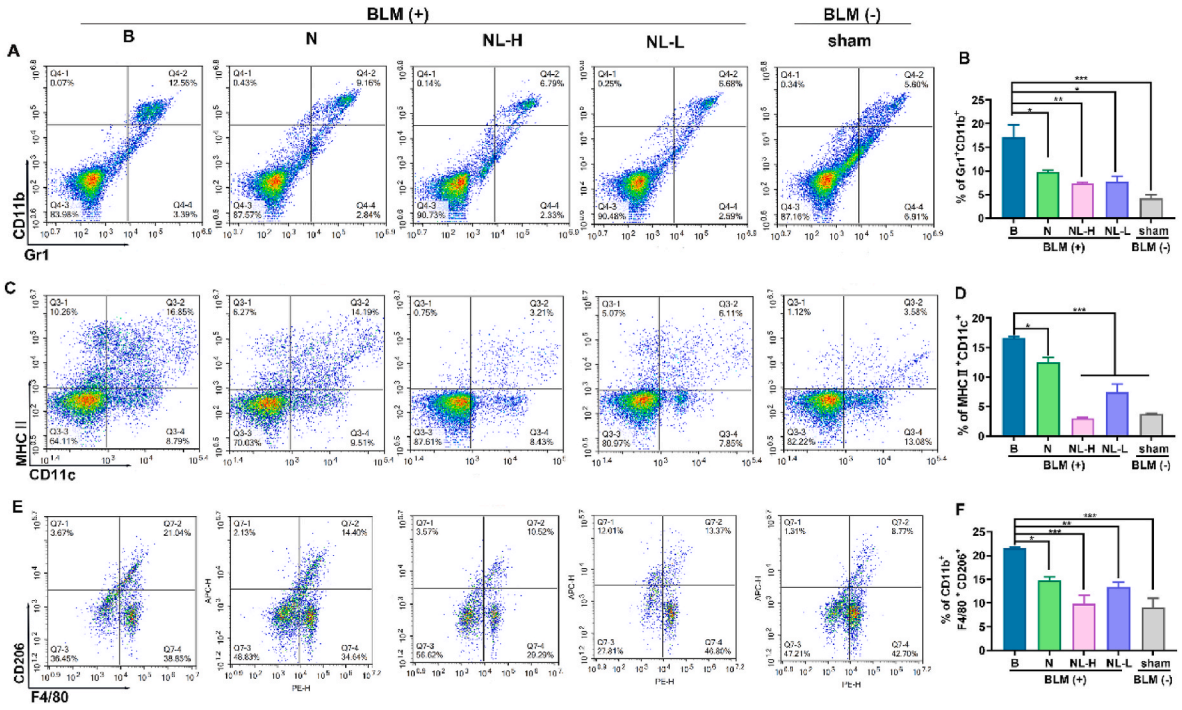

Fig. 4. Ncl-Lips improved the immune microenvironment in a BLM-induced lung fibrosis model. (A) Single-cell suspensions from the lungs of mice in each group were analyzed using flow cytometry to determine the presence of Gr1+CD11b+ (A, B), MHC II + CD11c+ (C, D) and CD11b + F4/80+CD206+ (E, F) cells. All the data are shown as the means ± SDs of three mice per group; $*P < 0.05$, $**P < 0.01$, and $***P < 0.001$.

morphology and lipid bilayer structure of the blank Lips and Ncl-Lips. The zeta potentials of blank-lips and Ncl-Lips were −9.25 ± 1.48 mV and −13.5 ± 0.98 mV respectively (Fig. 2B). These negatively charged results suggested that Ncl-Lips have good blood compatibility [30]. The average particle sizes of the blank-lips and Ncl-Lips were determined to be 119.60 ± 2.20 nm and 136.97 ± 0.54 nm, respectively, with a polydispersity index (PDI) of 0.14–0.17 (Fig. 2C and D). Notably, the fabricated Ncl-Lips exhibit stability when stored at 4 °C for at least 15 days, as evidenced by the lack of significant changes in size or PDI (Table S1). We found that the original sample still had a Tyndall effect after six months of storage at 4 °C (Figure S2A). The Ncl-Lips were determined to be 173.9 ± 6.172 nm in length and to have a PDI of 0.186 ± 0.01 (Figure S2B). This formulation has shown excellent stability. In addition, the EE of Ncl-Lips was 89.49% ± 2.40%, while that of Ncl-Lips was as high as 32.25% ± 0.49%. The mass concentration of Ncl in every batch of prepared Ncl-Lips was approximately 1 mg/mL. More drug loading was found than that in our previous study [18]. This may also explain why the space enclosed in liposomes is much larger than that available in micelles [31]. As presented in Fig. 2E, comparison of the photograghs of the three samples showed that the water solubility of Ncl improved. The UV–vis absorption spectra of Ncl, blank lips and Ncl-Lips were examined for characteristic absorption at 332 nm for Ncl, demonstrating that Ncl was loaded into the liposomes (Fig. 2F). Importantly, as illustrated in Fig. 2G, the cumulative release of Ncl in the Ncl group markedly increased compared with that the Ncl-Lips group before 24 h. Moreover, Ncl-Lips exhibited a slow cumulative release behavior. The presence of Ncl-Lips indicated that liposomes nanocarriers had the advantage of extended drug release. Therefore, these results indicated that Ncl-Lips could be well-dispersed and easy to prepare, stable, and had high water-solubility and sustained drug release properties.

3.2. The therapeutic effect of Ncl-Lips on BLM-induced pulmonary fibrosis

To investigate whether Ncl-Lips has a therapeutic effect on pulmonary fibrosis, a bleomycin-induced pulmonary fibrosis mouse model was generated. This model was established by the American Thymus Association (ATS) and is the most extensive first-line mouse pulmonary fibrosis model of IPF [32]. During this study, male C57BL/6 mice at approximately 8 weeks of age were given an intratracheal infusion of bleomycin (~2 mg/kg). After 10 days, the pulmonary inflammation gradually subsided, fibrosis occurred, and the drug was administered every two days intervals. Ncl (5 mg/kg) was administered intraperitoneally and Ncl-Lips or blank Lips were administered by intravenous injection until Day 21 (Fig. 3A). To evaluate the effect of Ncl-Lips on the structure of mouse lung tissue, histological staining techniques involving H&E and Masson were employed to examine pathological sections of the lung tissues. H&E staining demonstrated that, in comparison to those in the sham group, the alveolar space in the Ncl-Lips group collapsed and thickened after bleomycin injection, and the destruction of the lung structure was accompanied by the deposition of fibrocyte foci (Fig. 3B); moreover, the Ncl-Lips group showed more obvious structural improvement than the Ncl group. The results were histologically assessed using the Ascroft score (Fig. 3C). In addition, collagen formation in pulmonary fibrosis was detected by Masson staining and hydroxyproline content in lung tissue. Consistent with the H&E results, BLM-treated mice exhibited showed significant collagen deposition (Fig. 3B–D, E). Both Ncl and Ncl-Lips significantly downregulated bleomycin-induced collagen production (Fig. 3E). These data indicate that Ncl-Lips can significantly alleviate the advancement of pulmonary fibrosis. In addition to the detection of collagen in tissues, other indicators of myofibroblast activation, including the expression of collagen I, α-SMA and vimentin in lung tissues, were also detected via Western blot analysis. The collagen I, α-SMA and vimentin proteins were upregulated under bleomycin induction, while the E-cadherin proteins were downregulated. Compared with that in the BLM + Lips group, the administration of 2 mg/kg Ncl-Lips (NL-H) downregulated collagen I, α-SMA and vimentin (Fig. 3F–H, Figure S3).

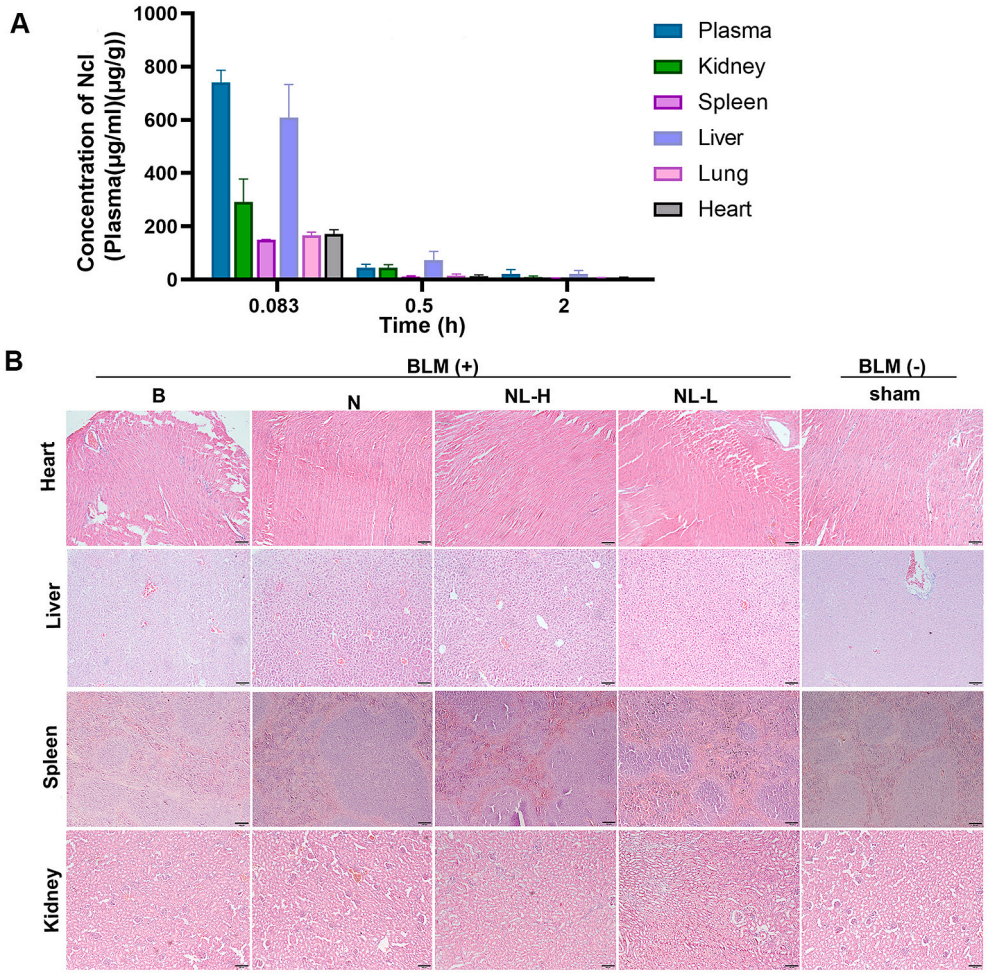

Fig. 5. Pharmacokinetic profile, tissue distribution and toxicity of Ncl-Lips. (A) Plasma concentration and tissue distribution time profiles of Ncl after intravenous (*i.v.*) injection Ncl-Lips. All the data are shown as means ± SDs, n = 3. (B) Representative H&E staining images of heart, liver, spleen and kidney sections from the indicated groups of mice. Scale bar: 100 μm.

3.3. Ncl-Lips improved the immune microenvironment in BLM-induced pulmonary fibrosis

The regulatory function of immune cells in early inflammation and late damage repair is a significant contributor to the pathogenesis of pulmonary fibrosis [33]. Therefore, flow cytometry was also used to determine the composition of lung immune cells in fibrotic mice treated with Ncl-Lips. As shown in Fig. 4, bleomycin significantly increased the proportion of lung myeloid suppressor cells (MDSCs, Gr1+CD11b+), dendritic cells (DCs, MHCII + CD11c+) and macrophages (F4/80+CD11b + CD206+). Interestingly, NL-H group (Ncl-Lips, 2 mg/kg) reduced the accumulation of these immune cells. The BLM-treated group exhibited an average of 13.85% Gr1+CD11b + cells and 15.76% MHCII + CD11c + cells, whereas the sham group had percentages of 5.33% and 3.73%, respectively (Fig. 4). In contrast, the Gr1+CD11b + cells and MHCII + CD11c + cells were notably lower in the Ncl-Lips group than BLM-treated group, with an average of 3.82% and 3.04%, respectively, and an average of 7.15% and 12.70%, respectively, in the Ncl group (5 mg/kg) (Fig. 4A–D). These findings suggested that Ncl-lips may ameliorate immune microenvironment imbalance [34].

On the basis of our previous reports, M2 macrophages (CD11b + F4/80+CD206+) secrete TGFβ1 and other fibrotic cytokines involved in fibrosis progression [15]. Subsequently, the impact of Ncl-Lips on M2 macrophages *in vivo* was investigated. As shown in Fig. 4E, F, there was revealed that an average of 21.50% CD11b + F4/80+CD206+ cells in the BLM-treated group vs. 9.00% in the sham group. The Ncl-Lips group exhibited a significant reduction in the percentage of CD11b + F4/80+CD206+ cells at a dose of 2 mg/kg, with an average of 9.80% in the Ncl-Lips group, and an average of 13.50% in the Ncl group (5 mg/kg) (Fig. 4 E, F). We confirmed that Ncl-Lips may possess the ability to repair the damaged immune microenvironment. Moreover, the latest review described the use of nanoparticle-based drug delivery systems for pulmonary diseases [35]. Our results confirmed the advantage of liposomes nanoparticles for the treatment of PF.

3.4. Pharmacokinetic profile, tissue distribution and toxicity of Ncl-Lips

In addition to the efficacy of PF on Ncl-Lips, the pharmacokinetic profile, tissue distribution and safety of Ncl-Lips *in vivo* were evaluated. We mainly examined the distribution of Ncl-Lips in plasma and major organs, including the lungs. After intravenous administration to SD rats. Tissue samples were collected at various temporal intervals and the concentration of Ncl-Lips was detected via UPLC−MS/MS (Table S2 and Fig. 5A). Although Ncl-Lips are most highly expressed in the plasma and liver, Ncl-Lips are still distributed in lung tissue and can reach lung tissue within a short time after administration. The highest blood concentration was reached at the time of the first sampling (0.083 h), indicating that the drug reached systemic circulation soon after intravenous administration. In contrast, in previous studies [36], the tissue distribution of Ncl was very limited, with markedly greater concentrations of Ncl in the intestine, kidneys, and liver after intravenous

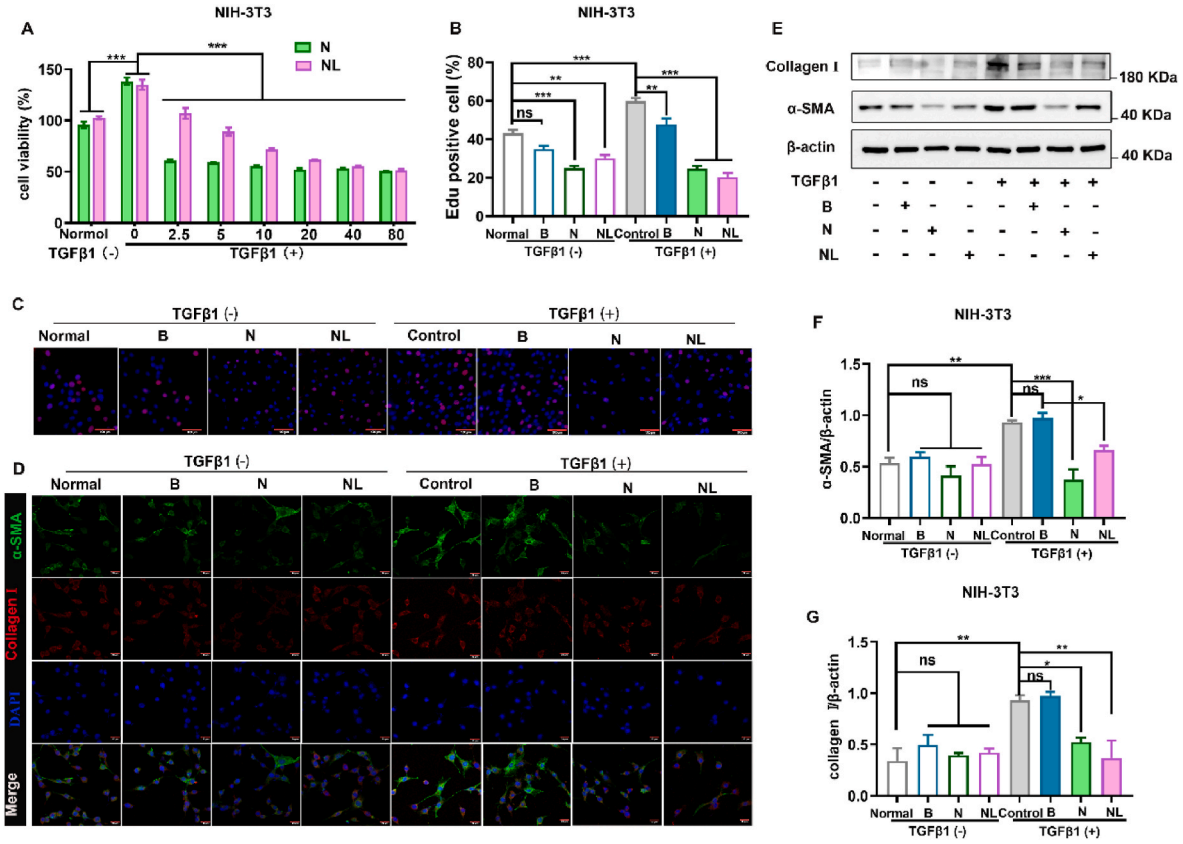

Fig. 6. Ncl-Lips inhibits TGFβ1-induced fibroblast activation. (A) According to CCK-8 assay, Ncl-Lips inhibited the proliferation of NIH-3T3 cells. The data are expressed as the mean ± SD. ***$P < 0.001$ vs. control. (B) Statistics of (C). (C) EdU and DAPI staining of NIH-3T3 cells. Scale bars: 100 μm. (D) Expressions of collagen I and a-SMA in fibroblasts following TGFβ1 stimulation with Ncl or Ncl-Lips for 24 h determined by immunofluorescence staining. The nuclei (blue) were stained with DAPI. Scale bar: 20 μm. (E–G) Western blot analysis (E) and statistical analysis of a-SMA (F) and collagen I (G) expression in fibroblasts after induction with TGFβ1 and Ncl or Ncl-Lips for 24 h. All the data are expressed as the means ± SDs. *$P < 0.05$, **$P < 0.01$, and ***$P < 0.001$. (For interpretation of the references to colour in this figure legend, the reader is referred to the Web version of this article.)

administration of Ncl (2 mg/kg) in rats than in other tissues, including the spleen, lungs, and heart.

Mice bearing PF were treated with different formulations and the main organs including the heart, kidney, liver, and spleen, of each experimental group were collected for toxicity assessments. H&E staining of the aforementioned organs of the treated mice revealed no significant lesions, as shown in Fig. 5B. Furthermore, we evaluated the differences in the serum biochemical indices, including aspartate transaminase (AST), alanine aminotransferase (ALT), total protein (TP2), uric acid (UA), high-density lipoprotein 3 (HDLC3) and high-density lipoprotein 4 (HDLC4) between the group of mice. There were no statistically significant differences observed between the groups of mice (Figure S4). Taken together, these results demonstrated the safety and biocompatibility of Ncl-Lips, which is an effective liposome-based delivery platform for PF therapy.

3.5. Ncl-Lips inhibits TGFβ1-induced fibroblast activation

Given that Ncl-Lips intervention affects the expression of fibrotic proteins in lung fibrosis, we further conducted *in vitro* experiments to explore the role of Ncl-Lips in the transformation of fibroblasts into myofibroblasts. We modeled fibroblast activation via TGFβ1 (5 ng/mL) stimulation in NIH-3T3 cells *in vitro*. The results showed that cell proliferation was significantly increased after TGFβ1 stimulation and increased by approximately 30% after 72 h (Fig. 6A). These results demonstrated that Ncl-Lips inhibited proliferation in a dose-dependent manner. EdU staining also confirmed that Ncl-Lips inhibited cell proliferation and TGFβ1-induced cell proliferation (Fig. 6B and C). Notably, although Ncl itself is more inhibitory than the other agents, this difference may be due to its own toxicity [15,37]. Figure S5 displays the inhibitory effect of Ncl-Lips on the normal LO2 and Vero cells. To compare the effects of Ncl-Lips and equivalent doses of Ncl on lung fibroblast transformation, we detected the levels of α-SMA, a marker of myoblast transformation, and collagen I, an extracellular matrix component secreted after transformation via immunofluorescence experiments on NIH-3T3 cells (Fig. 6D and Figure S6). After TGFβ1 stimulation, the expression of these proteins significantly increased, with the expression levels increasing approximately 3-fold and decreasing after Ncl-Lips (5 μg/mL) treatment, while Ncl treatment also had a significant inhibitory effect (Fig. 6E). Next, the expression levels of α-SMA and collagen I were detected via Western blotting (Fig. 6E–G). The results showed that TGFβ1 stimulation significantly increased the α-SMA and collagen I protein levels, which were reduced after Ncl-Lips treatment. When Ncl-Lips were added to TGFβ1, the increases in the of α-SMA and collagen I levels were reduced by 26% and 43% respectively (Fig. 6F). In conclusion, the above experimental data indicate that Ncl-Lips has a significant inhibitory effect on TGFβ1-induced fibroblast activation, and is safer than Ncl.

3.6. Ncl-Lips inhibits EMT in lung epithelial cells

The role of EMT is crucial in the pathogenesis of pulmonary fibrosis [38]. However, EMT is a complex process that involves various changes, such as cytoskeletal remodeling and reduced E-cadherin levels [18,39]. *In vivo* intervention with Ncl-Lips had an impact on the expression of vimentin and E-cadherin in the pulmonary tissues of mice afflicted with

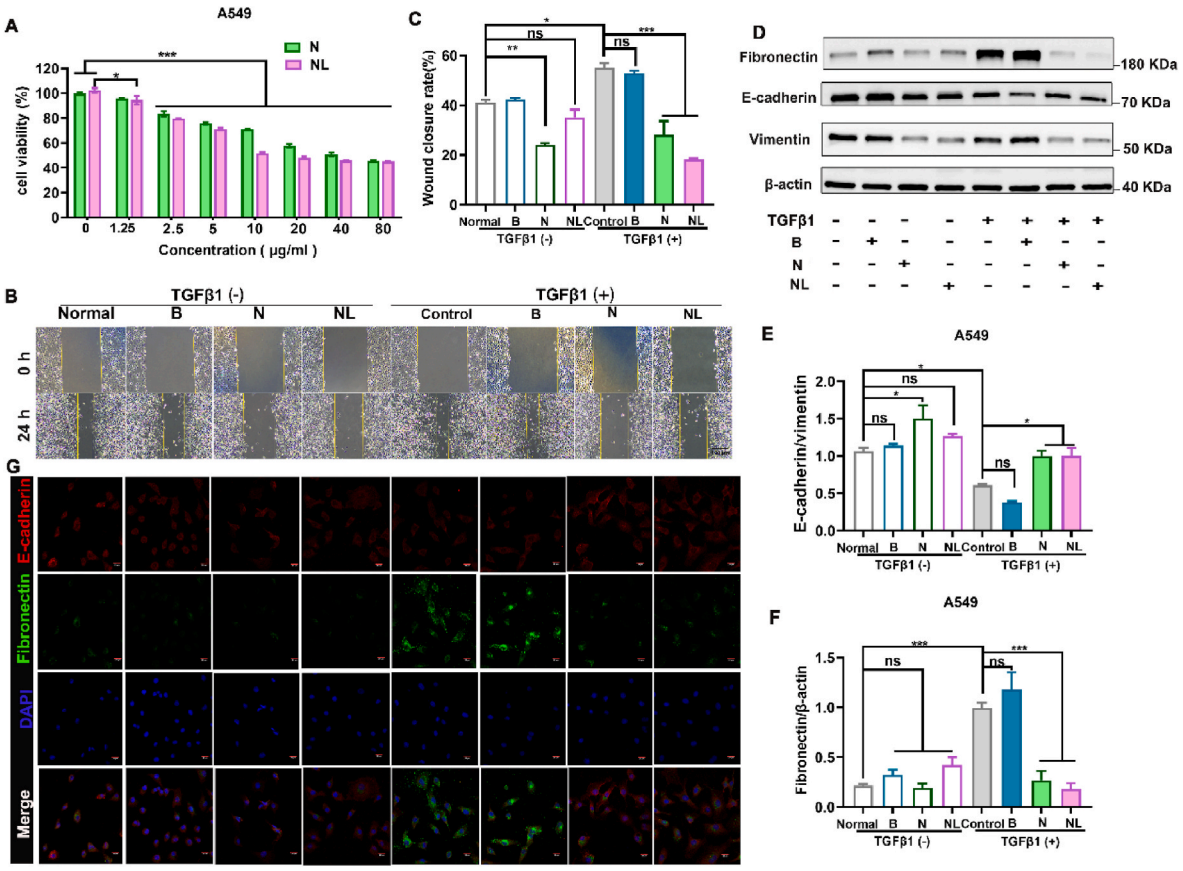

Fig. 7. The effect of Ncl-Lips on lung epithelial cells and the results of statistical analyses. (A) CCK-8 analysis showing inhibitory effect of Ncl-Lips on the proliferation of A549 cells. The data are expressed as the mean ± SD. $^{*}P < 0.05$, $^{***}P < 0.001$. (B, C) Representative images of migration assays (B) and quantification (C) of A549 cells treated with TGFβ1, Ncl-Lips or Ncl. Scale bar: 100 μm. The data are expressed as the mean ± SD. $^{*}P < 0.05$, $^{**}P < 0.01$, $^{***}P < 0.001$. (D–F) Western blot analysis of Vimentin, E-cadherin, Fibronectin and β-actin expression in A549 cells after TGFβ1 induction with Ncl or Ncl-Lips for 24 h. All the data are expressed as the means ± SDs. n = 3. $^{*}P < 0.05$, $^{***}P < 0.001$. (G) Representative images of E-cadherin and fibronectin immunostaining in A549 cells after TGFβ1 stimulation with Ncl or Ncl-Lips for 24 h. The nuclei (blue) were stained with DAPI. Scale bar: 20 μm. (For interpretation of the references to colour in this figure legend, the reader is referred to the Web version of this article.)

pulmonary fibrosis (Fig. 3F). To further confirm and investigate whether Ncl-Lips can inhibit EMT *in vitro*, A549 cells were treated with TGFβ1 to induce EMT [40]. First, the findings shown in Fig. 7A indicate that the proliferation of A549 cells was inhibited by Ncl-Lips. Subsequently, we observed that, compared to control cells, A549 cells induced by TGFβ1 had a more elongated mesenchymal phenotype and greater migration ability (Figure S7A). However, Ncl-Lips partially maintained epithelial cell morphology and blocked TGFβ1-induced cell migration by 63% (Fig. 7B and C). Similar to the *in vivo* results, the immunofluorescence and Western blotting results showed that TGFβ1 upregulated the protein levels of vimentin and fibronectin, and reduced the protein levels of E-cadherin proteins in A549 cells (Fig. 7D–G, Fig. S7B and C), indicating successful construction of the EMT model. Importantly, treatment with Ncl-Lips reversed the levels of the associated marker proteins. To further validate this conclusion, we generated additional BEAS-2B cells, which were treated with TGFβ1 to induce EMT. Figure S8 shows the results obtained. Collectively, these data collectively demonstrate that the use of Ncl-Lips as an effective nanomedicine could attenuate pulmonary fibrosis by inhibiting the EMT process.

4. Discussion

Pulmonary fibrosis has been recognized as is an uncommon and serious fatal lung disease in recent years. The number of cases has been increasing rapidly, especially in the elderly population, which is partly due to COVID-19, smoking and inflammation. Niclosamide (Ncl) is an old anthelmintic medicine, and destruction of mitochondrial metabolism has been observed in both parasitic and animal models. Recent research has indicated that Ncl can inhibit renal and liver fibrosis through the regulation of various signaling pathways [41,42]. Our finding demonstrated that the effect of administering micellar encapsulated Ncl on pulmonary fibrosis was more efficient than that of the other agents. However, this drug has low solubility and high permeability [15]. Each drug dosage form has advantages and disadvantages. However, our effort to optimize the formulation to enhance its therapeutic efficacy is appreciable [43]. Liposomes are promising drug delivery systems [44]. In the present study, the presence of Ncl-Lips indicated that liposomes might prevent unwanted Ncl leakage and have the advantage of low drug release (Fig. 2). Moreover, the results demonstrated that Ncl-Lips could enhance the efficacy of Ncl in a mouse model (Fig. 3). This evidence may lead to new ideas for clinical research and the utilization of Ncl. Therefore, efforts have been undertaken to improve the bioavailability of Ncl by using different kinds of nanoparticles [18].

Regarding the regulation of the lung immune environment by Ncl-Lips (Fig. 4), first, we and others have determined by FCM that the macrophages recruited in bleomycin-induced fibrotic lungs in mice, are predominantly M2 macrophages, and that M2 rather than M1 macrophages promote fibroblast differentiation and high α-SMA expression [15,45]. Therefore, we evaluated the changes in M2-type macrophages in the PF of mice. In addition, inhibiting the recruitment of mature DCs to the lungs can reduce the occurrence of chronic inflammation in the

lungs, consequently diminishing the activation of myofibroblasts and the process of extracellular matrix accumulation [46]. Finally, there is no doubt that T cells are engaged in the progression of fibrosis, but the underlying mechanism is complex. In general, the profibrotic or anti-fibrotic role of T cells in PF varies with T-cell subset and pathological stage [47]. Our results showed that Ncl-Lips could reduce the accumulation of these immune cells (Gr1+CD11b+, MHC II + CD11c+ and M2 macrophages). These findings suggested that Ncl-lips may ameliorate immune microenvironment imbalances, and that they also have good anti-pulmonary fibrosis effects, providing a basis for further clinical research.

In this study, a mouse model of BLM-induced pulmonary fibrosis was generated. Initially, we evaluated the ability of Ncl-Lips to reverse of pulmonary fibrosis. Furthermore, our research revealed that Ncl-Lips can impede the activation of fibroblasts and the process of EMT in lung epithelial cells. As expected, the findings of this study verified that Ncl-Lips have the potential to enhance the efficiency of Ncl utilization in mice. Therefore, the required dosage and associated side effects may be reduced during *in vivo* administration. An important and significant finding in this study was that Ncl-Lips may have a prominent ability to repair the damaged immune microenvironment. Furthermore, the use of Ncl-Lips as an effective nanomedicine has demonstrated potential for mitigating pulmonary fibrosis through the inhibition of the EMT process.

5. Conclusions

We constructed niclosamide-encapsulated lipid nanoparticles (Ncl-Lips) for the reversal of pulmonary fibrosis. The released Ncl could inhibit fibrosis, consequently reversing the levels of the associated marker protein, inhibiting EMT in lung epithelial cells and improving the immune microenvironment, which is good for rebuilding normal lung architecture. Therefore, Ncl-Lips had good effects on an animal model of pulmonary fibrosis induced by bleomycin (BLM). These findings indicate that Ncl-Lips is an efficient drug-delivery agent for reversing pulmonary fibrosis.

CRediT authorship contribution statement

Yan Yu: Conceptualization, Data curation, Formal analysis, Funding acquisition, Investigation, Methodology, Project administration, Resources, Software, Supervision, Validation, Visualization, Writing – original draft, Writing – review & editing. **Hongyao Liu:** Data curation, Formal analysis, Investigation, Methodology, Software, Validation, Visualization, Writing – original draft. **Liping Yuan:** Investigation, Methodology. **Meng Pan:** Investigation, Methodology. **Zhongwu Bei:** Methodology. **Tinghong Ye:** Conceptualization, Funding acquisition, Project administration, Supervision, Validation, Writing – review & editing. **Zhiyong Qian:** Conceptualization, Funding acquisition, Supervision, Writing – review & editing.

Declaration of competing interest

The authors declare that they have no known competing financial interests or personal relationships that could have appeared to influence the work reported in this paper.

Data availability

Data will be made available on request.

Acknowledgments

This work was supported by the Foundation of Science and Technology Department of Sichuan Province (NO.2022NSFSC1465, 2023NSFSC0525), Post-Doctor Research Project, West China Hospital, Sichuan University (NO.2021HXBH086), the Sichuan University post-doctoral interdisciplinary Innovation Fund (NO.10822041A2118) and Full-Time Postdoctoral Research Fund of Sichuan University (NO. 20826041F4134). We also thank Sichuan Greentech Bioscience Co., Ltd. for their assistance in the Pharmacokinetic profile, tissue distribution of Ncl-Lips.

Appendix A. Supplementary data

Supplementary data to this article can be found online at https://doi.org/10.1016/j.mtbio.2024.100980.

References

[1] G. Huang, J. Liang, K. Huang, X. Liu, F. Taghavifar, C. Yao, T. Parimon, N. Liu, K. Dai, A. Aziz, Y. Wang, R.T. Waldron, H. Mou, B. Stripp, P.W. Noble, D. Jiang, Basal cell–derived WNT7A promotes fibrogenesis at the fibrotic niche in idiopathic pulmonary fibrosis, Am. J. Respir. Cell Mol. Biol. 68 (2022) 302–313, https://doi.org/10.1165/rcmb.2022-0074OC.

[2] L. Richeldi, H.R. Collard, M.G. Jones, Idiopathic pulmonary fibrosis, Lancet 389 (2017) 1941–1952, https://doi.org/10.1016/S0140-6736(17)30866-8.

[3] Z. Li, Q. Zhang, J. Xiang, M. Zhao, Y. Meng, X. Hu, T. Li, Y. Nie, H. Sun, T. Yan, Z. Ao, D. Han, Novel strategy of combined interstitial macrophage depletion with intravenous targeted therapy to ameliorate pulmonary fibrosis, Mater. Today Bio 20 (2023) 100653, https://doi.org/10.1016/j.mtbio.2023.100653.

[4] M. Casas, Air pollution exposure and interstitial lung diseases: have we identified all the harmful environmental exposures? Thorax 74 (2019) 1013, https://doi.org/10.1136/thoraxjnl-2019-213805.

[5] J.E. Michalski, J.S. Kurche, D.A. Schwartz, From ARDS to pulmonary fibrosis: the next phase of the COVID-19 pandemic? Transl. Res. 241 (2022) 13–24, https://doi.org/10.1016/j.trsl.2021.09.001.

[6] P.-U.C. Dinh, D. Paudel, H. Brochu, K.D. Popowski, M.C. Gracieux, J. Cores, K. Huang, M.T. Hensley, E. Harrell, A.C. Vandergriff, A.K. George, R.T. Barrio, S. Hu, T.A. Allen, K. Blackburn, T.G. Caranasos, X. Peng, L.V. Schnabel, K.B. Adler, L.J. Lobo, M.B. Goshe, K. Cheng, Inhalation of lung spheroid cell secretome and exosomes promotes lung repair in pulmonary fibrosis, Nat. Commun. 11 (2020) 1064, https://doi.org/10.1038/s41467-020-14344-7.

[7] M. Xu, E.M. Lee, Z. Wen, Y. Cheng, W.-K. Huang, X. Qian, J. Tcw, J. Kouznetsova, S.C. Ogden, C. Hammack, F. Jacob, H.N. Nguyen, M. Itkin, C. Hanna, P. Shinn, C. Allen, S.G. Michael, A. Simeonov, W. Huang, K.M. Christian, A. Goate, K. J. Brennand, R. Huang, M. Xia, G.-l. Ming, W. Zheng, H. Song, H. Tang, Identification of small-molecule inhibitors of Zika virus infection and induced neural cell death via a drug repurposing screen, Nat. Med. 22 (2016) 1101–1107, https://doi.org/10.1038/nm.4184.

[8] J. Tam, T. Hamza, B. Ma, K. Chen, G.L. Beilhartz, J. Ravel, H. Feng, R.A. Melnyk, Host-targeted niclosamide inhibits C. difficile virulence and prevents disease in mice without disrupting the gut microbiota, Nat. Commun. 9 (2018) 5233, https://doi.org/10.1038/s41467-018-07705-w.

[9] T. Sultana, U. Jan, J.I. Lee, Double Repositioning, Veterinary antiparasitic to human anticancer, Int. J. Mol. Sci. 23 (2022) 4315, https://doi.org/10.3390/ijms23084315.

[10] R. Kumar, L. Coronel, B. Somalanka, A. Raju, O.A. Aning, O. An, Y.S. Ho, S. Chen, S.Y. Mak, P.Y. Hor, H. Yang, M. Lakshmanan, H. Itoh, S.Y. Tan, Y.K. Lim, A.P. C. Wong, S.H. Chew, T.H. Huynh, B.C. Goh, C.Y. Lim, V. Tergaonkar, C.F. Cheok, Mitochondrial uncoupling reveals a novel therapeutic opportunity for p53-defective cancers, Nat. Commun. 9 (2018) 3931, https://doi.org/10.1038/s41467-018-05805-1.

[11] Y. Zhu, W. Zuo, L. Chen, S. Bian, J. Jing, C. Gan, X. Wu, H. Liu, X. Su, W. Hu, Y. Guo, Y. Wang, T. Ye, Repurposing of the anti-helminthic drug niclosamide to treat melanoma and pulmonary metastasis via the STAT3 signaling pathway, Biochem. Pharmacol. 169 (2019) 113610, https://doi.org/10.1016/j.bcp.2019.08.012.

[12] T. Ye, Y. Xiong, Y. Yan, Y. Xia, X. Song, L. Liu, D. Li, N. Wang, L. Zhang, Y. Zhu, J. Zeng, Y. Wei, L. Yu, The anthelmintic drug niclosamide induces apoptosis, impairs metastasis and reduces immunosuppressive cells in breast cancer model, PLoS One 9 (2014) e85887, https://doi.org/10.1371/journal.pone.0085887.

[13] M.S. Zeyada, N. Abdel-Rahman, A. El-Karef, S. Yahia, I.M. El-Sherbiny, L.A. Eissa, Niclosamide-loaded polymeric micelles ameliorate hepatocellular carcinoma in vivo through targeting Wnt and Notch pathways, Life Sci. 261 (2020) 118458, https://doi.org/10.1016/j.lfs.2020.118458.

[14] J. Xu, P.-Y. Shi, H. Li, J. Zhou, Broad spectrum antiviral agent niclosamide and its therapeutic potential, ACS Infect. Dis. 6 (2020) 909–915, https://doi.org/10.1021/acsinfecdis.0c00052.

[15] C. Gan, Y. Wang, Z. Xiang, H. Liu, Z. Tan, Y. Xie, Y. Yao, L. Ouyang, C. Gong, T. Ye, Niclosamide-loaded nanoparticles (Ncl-NPs) reverse pulmonary fibrosis in vivo and in vitro, J. Adv. Res. (2022), https://doi.org/10.1016/j.jare.2022.10.018.

[16] S. Singh, A.A.-O. Weiss, J.A.-O. Goodman, M.A.-O. Fisk, S.A.-O.X. Kulkarni, I.A.-O. Lu, J. Gray, R.A.-O. Smith, M.A.-O. Sommer, J.A.-O. Cheriyan, Niclosamide-A promising treatment for COVID-19, Br. J. Pharmacol. Chemother. 179 (2022) 3250–3267, https://doi.org/10.1111/bph.15843.

[17] R. Boyapally, G. Pulivendala, S. Bale, C. Godugu, Niclosamide alleviates pulmonary fibrosis in vitro and in vivo by attenuation of epithelial-to-mesenchymal transition,

matrix proteins & Wnt/β-catenin signaling: a drug repurposing study, Life Sci. 220 (2019) 8–20, https://doi.org/10.1016/j.lfs.2018.12.061.
[18] C. Gan, Q. Zhang, H. Liu, G. Wang, L. Wang, Y. Li, Z. Tan, W. Yin, Y. Yao, Y. Xie, L. Ouyang, L. Yu, T. Ye, Nifuroxazide ameliorates pulmonary fibrosis by blocking myofibroblast genesis: a drug repurposing study, Respir. Res. 23 (2022) 32, https://doi.org/10.1186/s12931-022-01946-6.
[19] H. Wanas, H.M. Elbadawy, M.A. Almikhlafi, A.E. Hamoud, E.N. Ali, A.M. Galal, Combination of niclosamide and pirfenidone alleviates pulmonary fibrosis by inhibiting oxidative stress and MAPK/Nf-κB and STATs regulated genes, Pharmaceuticals 16 (2023) 697, https://doi.org/10.3390/ph16050697.
[20] L. Sang, X. Guo, H. Fan, J. Shi, S. Hou, Q. Lv, Mesenchymal stem cell-derived extracellular vesicles as idiopathic pulmonary fibrosis microenvironment targeted delivery, Cells 11 (2022) 2322, https://doi.org/10.3390/cells11152322.
[21] M.O. Jara, Z.N. Warnken, R.O. Williams, Amorphous solid dispersions and the contribution of nanoparticles to in vitro dissolution and in vivo testing: niclosamide as a case study, Pharmaceutics 13 (2021) 97, https://doi.org/10.3390/pharmaceutics13010097.
[22] M.M.T. van Leent, B. Priem, D.P. Schrijver, A. de Dreu, S.R.J. Hofstraat, R. Zwolsman, T.J. Beldman, M.G. Netea, W.J.M. Mulder, Regulating trained immunity with nanomedicine, Nat. Rev. Mater. 7 (2022) 465–481, https://doi.org/10.1038/s41578-021-00413-w.
[23] M. Souri, M. Soltani, F. Moradi Kashkooli, M. Kiani Shahvandi, Engineered strategies to enhance tumor penetration of drug-loaded nanoparticles, J. Contr. Release 341 (2022) 227–246, https://doi.org/10.1016/j.jconrel.2021.11.024.
[24] N. Filipczak, J. Pan, S.S.K. Yalamarty, V.P. Torchilin, Recent advancements in liposome technology, Adv. Drug Deliv. Rev. 156 (2020) 4–22, https://doi.org/10.1016/j.addr.2020.06.022.
[25] H. Wu, M. Yu, Y. Miao, S. He, Z. Dai, W. Song, Y. Liu, S. Song, E. Ahmad, D. Wang, Y. Gan, Cholesterol-tuned liposomal membrane rigidity directs tumor penetration and anti-tumor effect, Acta Pharm. Sin. B 9 (2019) 858–870, https://doi.org/10.1016/j.apsb.2019.02.010.
[26] M. Dymek, E. Sikora, Liposomes as biocompatible and smart delivery systems – the current state, Adv. Colloid Interface Sci. 309 (2022) 102757, https://doi.org/10.1016/j.cis.2022.102757.
[27] J. Wang, M. Zhu, G. Nie, Biomembrane-based nanostructures for cancer targeting and therapy: from synthetic liposomes to natural biomembranes and membrane-vesicles, Adv. Drug Deliv. Rev. 178 (2021) 113974, https://doi.org/10.1016/j.addr.2021.113974.
[28] G. Wang, H. Gaikwad, M.K. McCarthy, M. Gonzalez-Juarrero, Y. Li, M. Armstrong, N. Reisdorph, T.E. Morrison, D. Simberg, Lipid nanoparticle formulation of niclosamide (nano NCM) effectively inhibits SARS-CoV-2 replication in vitro, Precis Nanomed 4 (2021) 724–737, https://doi.org/10.33218/001c.18813.
[29] Y. Yang, D. Hu, Y. Lu, B. Chu, X. He, Y. Chen, Y. Xiao, C. Yang, K. Zhou, L. Yuan, Z. Qian, Tumor-targeted/reduction-triggered composite multifunctional nanoparticles for breast cancer chemo-photothermal combinational therapy, Acta Pharm. Sin. B 12 (2022) 2710–2730, https://doi.org/10.1016/j.apsb.2021.08.021.
[30] L. Qi, H. Han, M.-M. Han, Y. Sun, L. Xing, H.-L. Jiang, S.J. Pandol, L. Li, Remodeling of imbalanced extracellular matrix homeostasis for reversal of pancreatic fibrosis, Biomaterials 292 (2023) 121945, https://doi.org/10.1016/j.biomaterials.2022.121945.
[31] G. Bozzuto, A. Molinari, Liposomes as nanomedical devices, Int. J. Nanomed. 10 (2015) 975–999, https://doi.org/10.2147/IJN.S68861.
[32] C. Lin, K. Borensztajn, C.A. Spek, Targeting coagulation factor receptors – protease-activated receptors in idiopathic pulmonary fibrosis, J. Thromb. Haemostasis 15 (2017) 597–607, https://doi.org/10.1111/jth.13623.
[33] S.J. Cho, H.W. Stout-Delgado, Aging and lung disease, Annu. Rev. Physiol. 82 (2020) 433–459, https://doi.org/10.1146/annurev-physiol-021119-034610.
[34] P.P. Mehta, V.S. Dhapte-Pawar, Repurposing drug molecules for new pulmonary therapeutic interventions, Drug Deliv. Transl. Res. 11 (2021) 1829–1848, https://doi.org/10.1007/s13346-020-00874-6.
[35] S. Pramanik, S. Mohanto, R. Manne, R.R. Rajendran, A. Deepak, S.J. Edapully, T. Patil, O. Katari, Nanoparticle-based drug delivery system: the magic bullet for the treatment of chronic pulmonary diseases, Mol. Pharm. 18 (2021) 3671–3718, https://doi.org/10.1021/acs.molpharmaceut.1c00491.
[36] M. Yang, A.Q. Wang, E.C. Padilha, P. Shah, N.R. Hagen, C. Ryu, K. Shamim, W. Huang, X. Xu, Use of physiological based pharmacokinetic modeling for cross-species prediction of pharmacokinetic and tissue distribution profiles of a novel niclosamide prodrug, Front. Pharmacol. 14 (2023), https://doi.org/10.3389/fphar.2023.1099425.
[37] F. Andrade, D. Rafael, M. Vilar-Hernández, S. Montero, F. Martínez-Trucharte, J. Seras-Franzoso, Z.V. Díaz-Riascos, A. Boullosa, N. García-Aranda, P. Cámara-Sánchez, D. Arango, M. Nestor, I. Abasolo, B. Sarmento, S. Schwartz, Polymeric micelles targeted against CD44v6 receptor increase niclosamide efficacy against colorectal cancer stem cells and reduce circulating tumor cells in vivo, J. Contr. Release 331 (2021) 198–212, https://doi.org/10.1016/j.jconrel.2021.01.022.
[38] M. Zhao, L. Wang, M. Wang, S. Zhou, Y. Lu, H. Cui, A.C. Racanelli, L. Zhang, T. Ye, B. Ding, B. Zhang, J. Yang, Y. Yao, Targeting fibrosis: mechanisms and clinical trials, Int. J. Software Tool. Technol. Tran. 7 (2022) 206, https://doi.org/10.1038/s41392-022-01070-3.
[39] M. Singh, N. Yelle, C. Venugopal, S.K. Singh, EMT: mechanisms and therapeutic implications, Pharmacol. Ther. 182 (2018) 80–94, https://doi.org/10.1016/j.pharmthera.2017.08.009.
[40] K. Muthuramalingam, M. Cho, Y. Kim, Cellular senescence and EMT crosstalk in bleomycin-induced pathogenesis of pulmonary fibrosis—an in vitro analysis, Cell Biol. Int. 44 (2020) 477–487, https://doi.org/10.1002/cbin.11248.
[41] Y. Li, C. Gan, Y. Zhang, Y. Yu, C. Fan, Y. Deng, Q. Zhang, X. Yu, Y. Zhang, L. Wang, F. He, Y. Xie, T. Ye, W. Yin, Inhibition of Stat3 signaling pathway by natural product pectolinarigenin attenuates breast cancer metastasis, Front. Pharmacol. 10 (2019), https://doi.org/10.3389/fphar.2019.01195.
[42] X. Pei, F. Zheng, Y. Li, Z. Lin, X. Han, Y. Feng, Z. Tian, D. Ren, K. Cao, C. Li, Niclosamide ethanolamine salt alleviates idiopathic pulmonary fibrosis by modulating the PI3K-mTORC1 pathway, Cells 11 (2022) 346, https://doi.org/10.3390/cells11030346.
[43] B. Ouyang, L. Deng, F. Yang, H. Shi, N. Wang, W. Tang, X. Huang, Y. Zhou, H. Yu, Y. Wei, J. Dong, Albumin-based formononetin nanomedicines for lung injury and fibrosis therapy via blocking macrophage pyroptosis, Mater. Today Bio 20 (2023) 100643, https://doi.org/10.1016/j.mtbio.2023.100643.
[44] H. Jin, M. Jeong, G. Lee, M. Kim, Y. Yoo, H.J. Kim, J. Cho, Y.-S. Lee, H. Lee, Engineered lipid nanoparticles for the treatment of pulmonary fibrosis by regulating epithelial-mesenchymal transition in the lungs, Adv. Funct. Mater. 33 (2023) 2209432, https://doi.org/10.1002/adfm.202209432.
[45] J. Hou, J. Shi, L. Chen, Z. Lv, X. Chen, H. Cao, Z. Xiang, X. Han, M2 macrophages promote myofibroblast differentiation of LR-MSCs and are associated with pulmonary fibrogenesis, Cell Commun. Signal. 16 (2018) 89, https://doi.org/10.1186/s12964-018-0300-8.
[46] S. Jeoung-Sook, Unexpected role of dendritic cells in pulmonary fibrosis, Thorax 74 (2019) 925, https://doi.org/10.1136/thoraxjnl-2019-213510.
[47] L. Deng, T. Huang, L. Zhang, T cells in idiopathic pulmonary fibrosis: crucial but controversial, Cell Death Dis. 9 (2023) 62, https://doi.org/10.1038/s41420-023-01344-x.